JOURNAL OF THEORETICAL AND APPLIED MECHANICS
44, 3, pp. 667-689, Warsaw 2006

MODELLING CREEP, RATCHETTING AND FAILURE IN STRUCTURAL COMPONENTS SUBJECTED TO THERMO-MECHANICAL LOADING

Fion P.E. Dunne

Department of Engineering Science, Oxford University, UK
e-mail: fionn.dunne@eng.ox.ac.uk

Jianguo Lin

Department of Mechanical and Manufacturing Engineering, University of Birmingham, UK
e-mail: j.lin@bham.ac.uk

David R. Hayhurst

John Makin

School of Mechanical, Aeronautical and Civil Engineering, University of Manchester, UK
e-mail: d.r.hayhurst@manchester.ac.uk

Experiments have been described in which copper components have been subjected to combined cyclic thermal and constant mechanical loading. Two thermal cycles were employed leading to predominantly cyclic plasticity damage and balanced creep – cyclic plasticity damage loading cycles. The combined loading led to component ratchetting and ultimately to failure.
Continuum damage-based finite element techniques have been developed for combined cyclic plasticity, creep and ratchetting in components subjected to thermo-mechanical loading. Cycle jumping techniques have been employed within the finite element formulation to minimise computer CPU times. The finite element methods have been used to predict the behaviour of the copper components tested experimentally and the results compared.
Steady-state ratchet rates were found to be well predicted by the models. Modes of failure and component lifetimes were also found to be reasonably well predicted. The experimental results demonstrate the importance of isotropic cyclic hardening on the initial component ratchetting rates.

Key words: creep damage, cyclic plasticity damage, thermo-mechanical loading, FE modelling, thermo-mechanical testing

1. Introduction

Over the last two decades, much effort has been devoted to the development of design criteria for structural components operating under extreme mechanical, thermal and environmental loading conditions, but it still remains a challenging problem. Components of this type arise, for example, in nuclear and conventional power plant, in pressure vessels and piping, and in aerospace applications (Blackman *et al.* 1983). Components that operate below the creep regime, may be subjected to regions of high stress which may be induced as a result of severe thermal gradients and mechanical loads, which may lead to the initiation and propagation of damage and micro–cracks due to cyclic plasticity (Remy and Skelton, 1990). Components that operate at high temperatures in the creep regime under cyclic mechanical or thermal loading may, in addition to the above, be subjected to time-dependent deformation and damage processes due to creep, which are dependent on a range of factors such as temperature, rate effects and mean stress (Blackman *et al.*, 1983).

At the material level the evolution of time-dependent creep damage and cyclic plasticity damage have been shown to interact (Blackman *et al.*, 1983; Inoue *et al.*, 1985; Lemaitre and Plumtree, 1979), leading to significant reductions in component lifetime. Because of this interaction it is not possible to make realistic predictions of material behaviour based on the analysis of the individual processes alone. Hence, material models have been developed over the past two decades based on sets of internal variables (Miller, 1979; Kujowski and Mróz, 1980; Bodner and Partoum, 1975; Liu and Krempl, 1979; Chaboche and Rousellier, 1983; Chaboche, 1987; Benallal and Ben Cheikh, 1987; Benallal and Marquis, 1987; Dunne and Hayhurst, 1992a; Dunne *et al.*, 1992), which represent creep and cyclic plasticity damage.

At the component level the evolution of creep and cyclic plasticity damage leads to material weakening, to stress redistribution, and eventually to material or component failure (Lemaitre and Chaboche, 1990). It is therefore important to be able to model the growth and interaction of creep and cyclic plasticity damage to enable the prediction of component lifetimes. This has been achieved through the advancement of single damage state variable theories developed at the materials level by Hayhurst (1972; 1973) and at the structural level, through the development of Continuum Damage Mechanics (CDM), by Hayhurst *et al.* (1984a,b) and for creep rupture in 3D welds (Hayhurst *et al.*, 2005a), and by Chaboche (1988) for cyclic plasticity.

Such analysis techniques for design have been developed for a wide range of structural components, including notched and cracked members in plane stress

(Hayhurst, 1973), plane strain (Hayhurst *et al.*, 1984a), and axisymmetric situations (Hayhurst *et al.*, 1984b); weldments (Hall and Hayhurst, 1991; Wang and Hayhurst, 1994) and creep crack growth (Hall *et al.*, 1996; Lesne and Chaboche, 1988) and for components subjected to combined mechanical and thermal loading.

More recently, Johanssan *et al.* (2005) have developed accurate modelling techniques for ratchetting under multiaxial stress states, which have been applied to cyclic loading of rail steel. Manonukul *et al.* (2005) have coupled a physically-based creep model with combined isotropic and kinematic hardening to examine cyclic plasticity and multiaxial creep in thermo-mechanical fatigue in which failure is dominated by creep damage evolution.

Due to high computational cost, these approaches could not be used for components subjected to large numbers of operating cycles over which creep and cyclic plasticity damage interact. To overcome this difficulty, some years ago Dunne and Hayhurst (1992b, 1994) developed cycle jumping techniques which enabled calculations to be performed in structures and components over many thousands of cycles of mechanical and thermal loading in the absence of incremental plastic straining or ratchetting. This development enabled large finite element calculations to be carried out using modest computer power (Dunne and Hayhurst, 1992b).

More recently, Lin, Dunne and Hayhurst (1997) extended this capability to enable the behaviour of structural components to be calculated when ratchetting takes place. They demonstrate the effectiveness of the technique by comparing the predictions made, using two different methods, of the behaviour of a thermally loaded copper slag tap. The first method involved Finite Element analysis of the slag tap component studied by Dunne and Hayhurst (1992b), and the second method involved the modelling of the same slag tap using a multi-bar equivalent of the minimum loading section of the tap. Following this approach Lin *et al.* (1997) showed very close agreement between the two methods, hence validating the multi-bar modelling method for zero mechanical load. They also predicted, using the multi-bar model, the ratchetting behaviour of a slag tap subjected to a superimposed mechanical load.

In this paper, continuum damage – based finite element models are described for the analysis of components undergoing creep, cyclic plasticity, and ratchetting under combined thermo-mechanical loading. Experimental tests on copper components are reported and the results compared with the predictions obtained using the finite element models. In the next section, the experimental tests are described.

2. Slag tap ratchetting test facility and thermal fields for cyclic plasticity dominated and balanced creep-cycle plasticity conditions

The experimental setup used to carry out ratchetting behaviour on model copper slag taps is discussed in this section. The model slag tap design is based on a previous design due to Dunne and Hayhurst (1992b) and reported in detail by Dunne *et al.* (1993) which was used to study thermal loading only in the absence of mechanical loads. The principal variant in the present design is the addition of a mechanical loading facility.

2.1. Copper slag tap specimen

The specimen design may be seen in Figure 1. To provide an indication of the scale, the diameter of the copper water cooling pipe is 12 mm, the width of the minimum cross-section is 70.2 mm, the width of the larger cross-section, defined by the parallel sides of the specimen, is 74.2 mm, and the width of the loading shanks which contain loading pins is 74.2 mm. The overall height of the specimen is 255 mm. The depth of the specimen close to and parallel with the water cooling pipe is 56 mm, and the larger cross-section parallel to the loading pins is 74.6 mm.

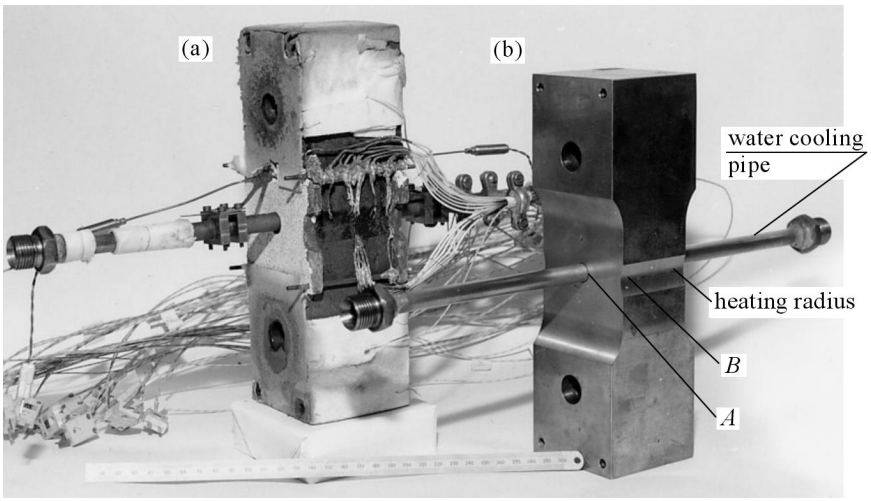

Fig. 1. Copper slag tap specimens with copper water cooling pipes thermally expanded into specimen, (a) thermocoupled temperature calibration specimen and (b) virgin specimen showing the locations of point A on the cooling duct and point B on the heating radius

The copper water cooling pipes are thermally expanded into the specimen by heating the specimens uniformly to 150°C and by cooling the pipes to liquid Nitrogen temperature. In this way an excellent mechanical contact is achieved which has good heat transfer properties. In practice, the cooling ducts are long relative to the width of the load bearing cross-sections, and so the conditions of stress approximate closely to those of plane strain. The ratio of specimen width to the water cooling pipe diameter is 70.2/12.0=5.6 hence justifying the existence of plane strain conditions.

2.2. Design and operation of the thermal loading facility

Heat is supplied to the specimen by means of two banks of three 500 W quartz line lamps, which are mounted symmetrically on either side of the specimen, and reflectors are used to direct heat onto the specimen. Each bank of three heaters and its reflector is supported by two heater support plates, which in turn are connected to the specimen load train by a parallelogram mechanism of linkages. The purpose of this mechanism is to ensure that as the specimen extends axially due to ratchetting, and the specimen width contracts, then the two heater banks move together in sympathy so ensuring that the heat radiation remains focussed on the specimen. Full details of experimental set-up are given by Hayhurst *et al.* (2005b). The steady test load is applied by a 100 kN servo-hydraulic testing machine.

The power output from the lamps (maximum total power of 2.25 kW) and the rate of flow of cooling water, are controlled by a programmable microprocessor, thus enabling the selected thermal loading history to be repeated accurately.

2.3. Establishment of thermal field histories

The objective of this research is to verify that it is possible to use viscoplastic constitutive equations, which embody the interactive evolution of combined cyclic plasticity and creep damage to predict, using continuum mechanics theories, the ratchetting behaviour which results from the damage interactions. Two areas are of principal interest. They are ratchetting with dominant cyclic plasticity damage, and ratchetting with balanced creep-cyclic plasticity damage. The types of thermal loading cycles required to achieve these are now discussed.

2.3.1. Cyclic plasticity damage dominated cycle

In order to achieve these conditions two requirements have to be met. Firstly, creep damage formation must be avoided and secondly, cyclic plasticity

damage is to be maximised. The former is achieved by maintaining specimen temperature below the creep regime, and if this cannot be completely achieved, then by reducing the time to a minimum for which testpiece temperatures enter the regime. The latter is achieved by maximising the temperature differences between the points A and B given in Figure 1 (and Figure 3, see later) at some point within the cycle. This has been brought about by maximising the cooling water flow rate whilst achieving optimum heat transfer conditions.

The selected thermal cyclic history is shown in Figure 2a. To avoid significant creep, temperatures are maintained below $300°\mathrm{C}$, and to maximise cyclic plasticity damage, a thermal down shock of $(\theta_B - \theta_A) = 86°\mathrm{C}$ has been achieved. The overall cycle time has been kept short so that the increment of cyclic plastic damage per cycle exceeds the contribution from creep damage. The details of the cycle are given as follows. Location B is maintained below $300°\mathrm{C}$ throughout the cycle. For time t in the range $0\,\mathrm{s} < t \leqslant 62.1\,\mathrm{s}$ heating is provided with no cooling; and, for $62.1\,\mathrm{s} < t \leqslant 92.1\,\mathrm{s}$ both heating and cooling are provided. The maximum temperature difference between A and B is $86°\mathrm{C}$ which occurs at 70.1 seconds. The overall cycle time is 92.1 seconds. The effectiveness of this selection will be verified by the results of the analysis presented later in the paper.

2.3.2. Balanced creep damage – cyclic plasticity damage cycle

To achieve this cycle the temperatures of the heating radius, point B in Figure 1 is permitted to fluctuate; but, in particular to exceed $300°\mathrm{C}$ and move well into the creep regime. In addition, the cycle contains a hold period of almost 300 seconds, at the temperature of $340°\mathrm{C}$ as shown in Figure 2b. It is these conditions which allow the creep damage to be similar in magnitude to the cyclic plasticity damage over the cycle. The details of the cycle are given as follows. For $0\,\mathrm{s} < t < 1308\,\mathrm{s}$ heating is provided with no cooling; for $1308\,\mathrm{s} < t < 1366.1\,\mathrm{s}$, both heating and cooling are provided; and for $1366.1\,\mathrm{s} < t \leqslant 1562.5\,\mathrm{s}$, cooling only is provided. The maximum temperature difference between A and B is $97.8°\mathrm{C}$, which occurs at 1366.1 seconds. The overall cycle time is 1562.5 seconds. Once again, the effectiveness of the chosen thermal condition will be verified by the results of the analysis presented later in the paper.

2.4. Application of mechanical load

The mechanical load was applied to the testpieces using a 100 kN servo-hydraulic test machine operated under load control. The testpieces shown in

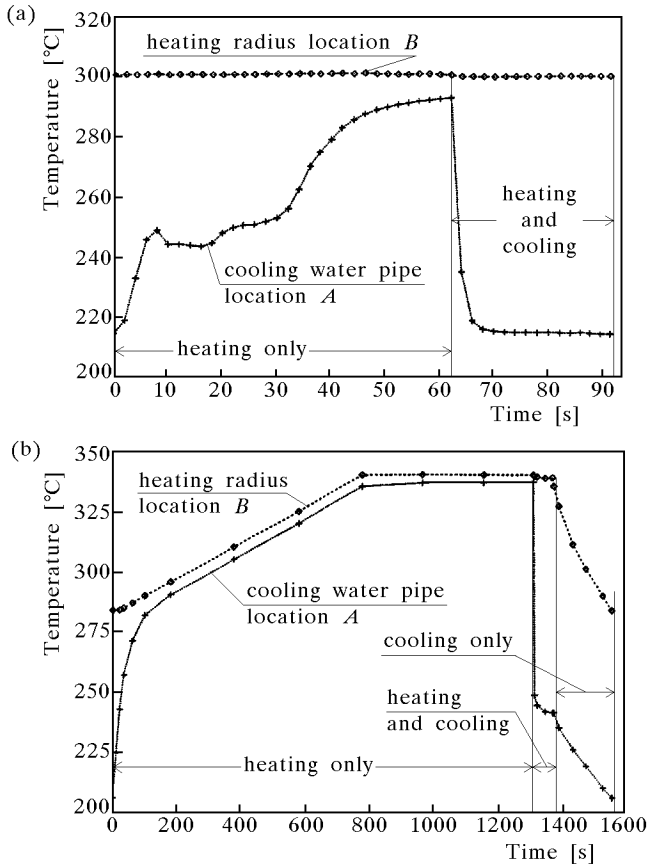

Fig. 2. Thermal histories at locations A and B defined in Figure 1 for (a) cyclic plasticity dominated cycle and (b) balanced creep-cyclic plasticity cycle

Figure 1 were connected to the testing machine load train through shear pins, which passed through the larger hole in the thicker section testpiece ends, and pinned the loading ties.

3. Constitutive equations

The elastic-viscoplastic damage constitutive equations employed in the present work are those described in detail elsewhere (Dunne and Hayhurst, 1992a, 1994) but for completeness, are summarised in Appendix A.

The total strain is given by ε, and the plastic and thermal strains by ε_p and ε_θ, respectively. The plastic strain rate term, $\dot{\varepsilon}_p$, given in (A.1) follows

from the normality hypothesis of plasticity with an appropriately defined viscoplastic potential. The internal variable, $\boldsymbol{x}$, models the kinematic hardening that occurs in cyclic viscoplasticity, and D is a scalar state variable representing combined irreversible material damage due to creep and cyclic plasticity. The material parameters K, n, C_i and γ_i are all temperature-dependent. The parameter k, in (A.1) is the cyclically hardened yield stress, and is dependent on both temperature and strain range. The physical basis for the temperature and strain range dependence of the cyclically hardened yield stress and of the temperature dependences in the constitutive equations is described in detail elsewhere (Lin *et al.*, 1996), where in addition, equations for the temperature sensitivities are given.

The scalar state variable, D, describing material damage in equations (A.1) to (A.3) is composed of damage due to creep and cyclic plasticity. The multi-axial form of the evolution equation for creep damage, ω, is given in the present formulation for creep-cyclic plasticity damage interaction (Dunne and Hayhurst, 1992a) in (A.4), where A, v and ϕ are temperature-dependent material parameters, σ_1 and σ_e are the maximum principal and effective stresses respectively, and α describes the multi-axial creep rupture criterion and the corresponding isochronous locus (Hayhurst, 1972). Here α has been assumed to take the value 0.7, reported by Hayhurst *et al.* (1984a) for commercially pure copper, and so the creep rupture behaviour is dominated by σ_1. The damage D_c contributes to the subsequent evolution of creep damage and is made up of contributions from the creep damage, and the cyclic plasticity damage. When cyclic plasticity damage is zero, as in the steady load creep, D_c becomes ω and it then represents the combined processes of cavity nucleation and growth as discussed by Greenwood (1973). The form of the interaction between creep and cyclic plasticity damage is described below.

The multi-axial equation employed for the evolution of cyclic plasticity damage evolution given in (A.5) is that proposed by Chaboche (1988), where A_{II} is the maximum effective stress range in a cycle, p is defined in terms of A_{II}, M is a function of mean stress, and β is a material parameter. Full details of the equations and of the methods used to determine the material parameters have been given by Dunne and Hayhurst (1992a, 1994).

The creep-cyclic plasticity damage interaction law proposed by Dunne and Hayhurst (1992a) is adopted here, and given in equations (A.6)-(A.9). The elastic viscoplastic damage constitutive equations for copper have been validated for conditions of creep, cyclic plasticity, and creep-plasticity interactions under both cyclic mechanical and cyclic thermal loading (Dunne and Hayhurst, 1992a, 1994). In addition, the material model has been employed successfully

to simulate the behaviour of a structural component subjected to cyclic thermal loading (Dunne and Hayhurst, 1992b) leading to cyclic plasticity. It is implemented into a finite element boundary and the initial value solver described elsewhere (Dunne and Hayhurst, 1992b). For uniaxial cyclic loading, the effect of damage on stress and viscoplastic strain rate is not considered in compression by setting $D = 0$, Eq. (A.8). This is used to model microcrack closure under compressive loading. For general multiaxial cases, the damage value is set to zero as the elemental hydrostatic stress becomes negative. The enhancement of the model to include the yield dependence on plastic strain range is described in the next section.

4. Finite element modelling of cyclically hardened yield stress k

The constitutive equations discussed above are based on the cyclically hardened stabilised state, in which the transient material behaviour that occurs over comparatively small numbers of cycles due to cyclic hardening is not modelled in detail. This enables economic computer analysis to be performed. The cyclically hardened yield stress, k, in the constitutive equation (A.1) includes two parts: the first is the initial yield stress, and the second is the isotropic hardening stress, which is related to the cyclic strain range as discussed by Lin *et al.* (1996). At the structural level, materials may be subjected to non-uniform stress and strain conditions. As a result, the cyclic strain range over the structure varies spatially, and the yield stress k varies accordingly. A problem therefore arises initially in that since pointwise strain ranges are not known a priori, it is not possible to determine the yield stress k. It is therefore necessary to develop a method to obtain the stabilised cyclically hardened yield stress field efficiently and to avoid modelling in detail the full transitional cycles necessary to achieve the isotropic hardened stress state. The method is described below.

Estimation of initial yield stress field

The determination of the yield stress field is equivalent to the evaluation of the strain range field for the component under strain controlled cyclic loading, since for a given temperature the yield stress is directly related to the cyclic strain range (Lin *et al.*, 1999). The initial cyclic strain range field is estimated according to the applied strain range and the distribution of ratios of elemental effective stress and volume averaged effective stress for the initial elastic solution.

The volume averaged elastic effective stress, Σ_{ev}, is defined by

$$\Sigma_{ev} = \sum_{i=1}^{n_e} \Sigma_i^e \frac{V_i^e}{n_e \sum_{i=1}^{n_e} V_i^e} \tag{4.1}$$

where n_e is the number of elements in the finite element mesh, Σ_i^e is the elemental effective stress for the ith element and V_i^e is the volume of the ith element. In order to estimate the cyclic strain range field, a factor F_i is introduced

$$F_i = \sqrt{\frac{\Sigma_i^e}{\Sigma_{ev}}} \qquad i = 1, 2, \ldots, n_e \tag{4.2}$$

The initial cyclic effective strain range field is obtained from

$$\Delta\varepsilon_i^e = F_i \Delta\varepsilon \qquad i = 1, 2, \ldots, n_e \tag{4.3}$$

where $\Delta\varepsilon_i^e$ is the estimated elemental cyclic strain range for the ith element, and $\Delta\varepsilon$ is the applied strain range for a strain-controlled cyclic loading test. Given the relationship between the yield stress and the cyclic strain range, the initial yield stress field can be estimated using the empirical relationship (Lin *et al.*, 1996), as

$$k_i = 153.3[1.139 - \exp(-1.319\Delta\varepsilon_i^e)] \exp(-2.0429 \cdot 10^{-3} T) \tag{4.4}$$

where $i = 1, 2, \ldots, n_e$ and k_i are the cyclic hardened elemental yield stresses, and T the temperature [K].

Subsequent yield stress field

The modelling of the first loading cycle is based on the yield stress field estimated above. The yield stress field for subsequent cycles is estimated from the effective strain range field obtained from the previous loading cycle and the initial estimated strain range field. Therefore, the subsequent effective strain field, $\Delta\varepsilon_e^{i,j+1}$, which is used for obtaining the yield stress field is estimated by

$$\Delta\varepsilon_e^{i,j+1} = \frac{1}{2}(\Delta\varepsilon_e^{i,j} + \Delta\varepsilon_e^{i,j-1}) \qquad i = 1, 2, \ldots, n_e \tag{4.5}$$

where $\Delta\varepsilon_e^{i,j}$ and $\Delta\varepsilon_e^{i,j-1}$ are the elemental effective strain ranges for the jth cycle and the $(j-1)$th cycle. The estimated effective strain range field, $\Delta\varepsilon_e^{i,j+1}$, can be used to calculate the yield stress field using Eq. (4.4) for the next cycle.

5. Cycle jumping in combined creep and cyclic plasticity

It is well known that the determination of lifetimes of structural components requires extremely long computer run times (Dunne and Hayhurst, 1994). In order to overcome this problem, a cycle jumping technique was developed and used for modelling deformation and failure behaviour to avoid the necessity of carrying out detailed calculations around all loading cycles, and yet maintaining the required solution accuracy. Cyclic plasticity tests carried out on cast copper (Dunne and Hayhurst, 1992b) have shown that material softening, due to creep and cyclic plasticity damage, does not have a significant effect on the load-carrying capacity or on the stress distribution within the material when the variation of the damage is small.

Therefore, a cycle jumping technique has been developed as follows. The cyclic behaviour of the stabilised stress, strain and yield stress is obtained by completing calculations over five full cycles. The resulting stress, strain and yield stress fields are then assumed to be constant, and only the creep damage and the cyclic plasticity damage are allowed to evolve and are integrated over a number of loading cycles according to the damage rates, $d\psi/dN$ and $d\omega/dN$. The number of cycles for which jumping takes place is limited in such a way that the increment of total damage for the element with the highest damage rate does not exceed 0.05, and individually the cyclic plasticity damage $\leqslant$ 0.014. These damage increments have been chosen empirically to ensure that the stress, strain and yield stress fields are not influenced significantly, and so that differences of the calculated lifetimes, for a uniaxial plane bar model, with and without the cycle jumping technique are $\leqslant 0.5\%$ for a wide range of temperature. The automatic selection of the number of cycles jumped and related numerical integration methods for the creep and plasticity damage were reported by Dunne and Hayhurst (1994). A cycle jump is allowed to take place, if possible, when every five full loading cycle calculations are completed. This ensures the stabilised stress, strain and yield stress fields can be obtained.

The cycle jumping method has been implemented into the finite element solver, Damage XX, to enable the rupture behaviour and lifetimes of cyclic plasticity testpieces to be modelled accurately and efficiently. For instance, in studies carried out for a uniaxial plane bar model, only 1/15 of the full cycle computation time is required if the cycle jumping technique is used at 20°C, with strain range 0.6% and strain rate 0.006% s^{-1}, and the difference in the number of cycles to failure with and without the cycle jumping method is approximately 0.2%.

6. Finite element analysis of components and comparison with experimental results

The copper component discussed above has been analysed using the continuum damage based finite element formulation presented above. The two cyclic thermal loading histories have been considered, together with the axial load applied. The component has been analysed in two dimensions under conditions of plane strain for reasons that will be discussed later. Because of the planes of symmetry, only a quadrant of the component needs to be considered for modelling purposes, and the finite element mesh employed is shown in Figure 3. Mesh sensitivity studies have been carried out for thermal and coupled thermal and mechanical loading analyses. A high density FE mesh was chosen for regions where stress and thermal gradients are high. Gradients were assessed by the maximum differences of stress and temperature in adjacent elements; and, the overall number of elements was limited by the CPU time. It was first necessary to establish the thermal field that the component was subjected to experimentally. A transient finite element analysis was carried out using as boundary conditions the experimental temperature variations at points A and B shown in Figure 2. The spatial variations of temperature with time were then obtained for both thermal cycles which were used as input to the mechanical analysis of the component. The component was in addition subjected to a constant axial load shown schematically in the finite element mesh in Figure 3. The results for the cyclic plasticity damage dominated cycle shown in Figure 2a are considered first, for which a constant mechanical stress of 30 MPa was applied.

6.1. Cyclic plasticity damage dominated cycle

Effective stresses have been calculated over a stabilised cycle, and the results are shown for these locations on the component in Figure 4. The effective stresses are shown (1) near to the cooling duct, (2) near the centre of the quadrant of the component shown in Figure 3, and (3) near the heating region. The results show that the highest effective stress occurs near the cooling duct. The rapid decrease in the stress that occurs at the beginning of the cycle results from the corresponding decrease in temperature difference shown in Figure 2a. The effective stresses at the cooling duct are smallest when the temperature difference is smallest. The stresses at the quadrant centre point remain fairly constant over the cycle reflecting the uniformity of the stress field in this vicinity generated by the applied constant stress of 30 MPa.

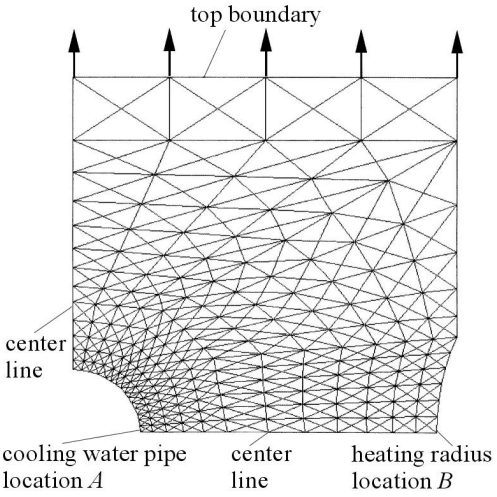

Fig. 3. Finite element mesh of the slag tap model used for the numerical analysis of the component under combined thermal and mechanical loading

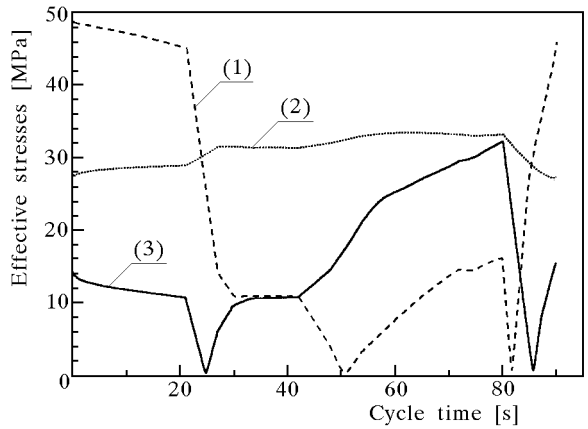

Fig. 4. Variation of effective stress over a stabilised cycle for the three locations (1) near the cooling duct, (2) the mid-point of the quadrant, and (3) near the heating region. The results are shown for the cyclic plasticity dominated cycle with an average applied stress of 30 MPa at the minimum section

Figure 5 shows the predicted and experimentally measured component displacement with the number of cycles. It should be noted that the predicted displacements are calculated as those occurring at the top boundary shown in Figure 3. The experimental displacements are measured over the full length of the specimen; that is, at the top and bottom component free surfaces just abo-

ve and below the sets of extensometer holes at the four extreme corners of the testpiece, as shown in Figure 1. However, because of the much larger sections of the component in the regions remote from the heating and cooling regions, the majority of the vertical strain occurs locally to these regions. For this reason, it is reasonable to assume that the displacements measured over the full length of the specimen are close to those that would be measured over the length corresponding to the finite element model in Figure 3, since the thicker parts of the testpiece are likely to be undergoing rigid body displacement only without significant straining.

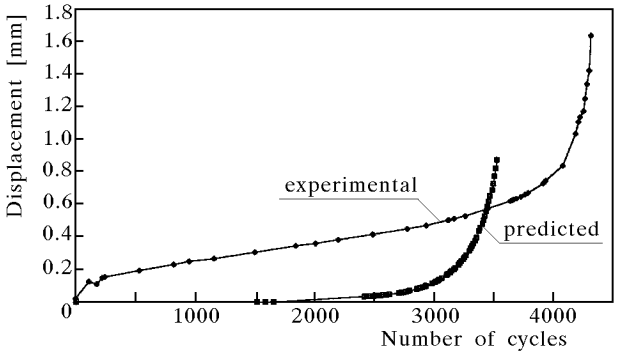

Fig. 5. Predicted and experimental variation of component loading direction displacement with cycles. The results are shown for the cyclic plasticity damage dominated cycle

The results show that very reasonable agreement in life (predicted: ~ 3500 cycles, experimental: $\sim$ 4300 cycles) is obtained, and in addition, that the steady-state ratchet rate is well predicted. The major difference in the results comes from the assumption in the model of an instantaneously fully-cyclically hardened state of the material. The transient process of cyclic hardening that occurs over the first 100 cycles in the material is ignored in the model. The consequence is that initially, the model assumes a much harder material than is actually the case, and therefore fails to predict the primary ratchetting that occurs over the first few cycles which leads to displacements of approximately 0.1 mm, shown in Figure 5. The overall quality of the prediction is therefore reasonable and the trend of the secondary and tertiary ratchetting is well predicted.

Figure 6 shows the variation of total strain in the loading direction with number of cycles at the heating radius and cooling duct. The strain can be seen to be the largest at the cooling duct with initially very low ratchet rates. The ratchet rates subsequently increase progressively with increasing levels

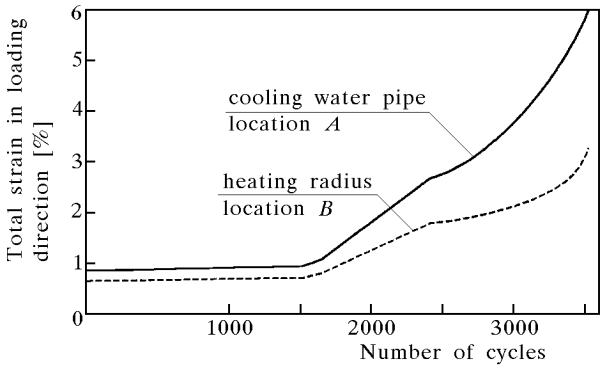

Fig. 6. Variation of total strain with number of cycles at locations A and B specified in Figure 3. The results are shown for the cyclic plasticity damage-dominated cycle

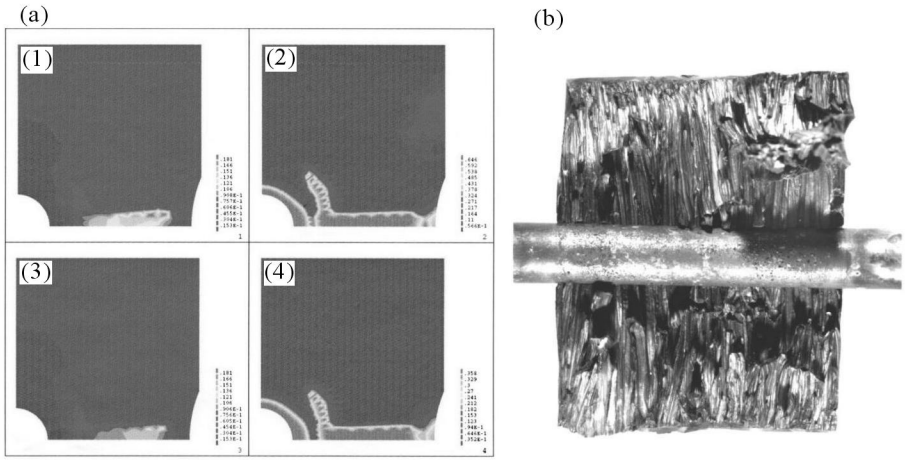

Fig. 7. (a) Predicted spatial variations of creep (1) and cyclic plasticity (2) damage at component failure and at a life fraction of 0.92, (3) and (4) respectively, shown for the cyclic plasticity damage-dominated cycle, and (b) failed slag tap (plan view) tested under an applied average mechanical stress of 30 MPa for the cyclic plasticity-dominated cycle, showing the fracture surface and chill-cast grain structure and stable cyclic plasticity damage evolution and crack growth

of damage. The distribution of damage predicted by the model can be seen in Figure 7a. The figure shows the creep and cyclic plasticity damages at failure ((1) and (2) respectively) and at a life fraction of 0.92 ((3) and (4) respectively). The comparatively low levels of creep damage at failure can be seen to occur removed from both the heating region and cooling duct, and to occur in the mid-section of the quadrant shown. This results from the strong

dependence of the creep damage rate on the maximum principal stress in copper. The maximum principal stresses remain fairly uniform and constant in the quadrant mid-section, leading to the creep damage shown. The cyclic plasticity damage initiates in three separate locations: at the cooling duct, at the heating radius, and at the quadrant mid-section. At failure the three zones of damage link leading to rupture along the component minimum section. This was observed in experiments, and an example is given in Figure 7b, which shows a plane view of the fracture surface, the chill-cast grain structure and stable cyclic plasticity damage evolution and crack growth through the testpiece minimum section.

6.2. Balanced creep and cyclic plasticity damage cycle

The thermal cycle corresponding to the generation of balanced creep and cyclic plasticity damage is shown in Figure 2b. The component is subjected to this cycle repeatedly, together with a constant applied mechanical stress of 25 MPa. The results of the analysis for these loading conditions are discussed in this section.

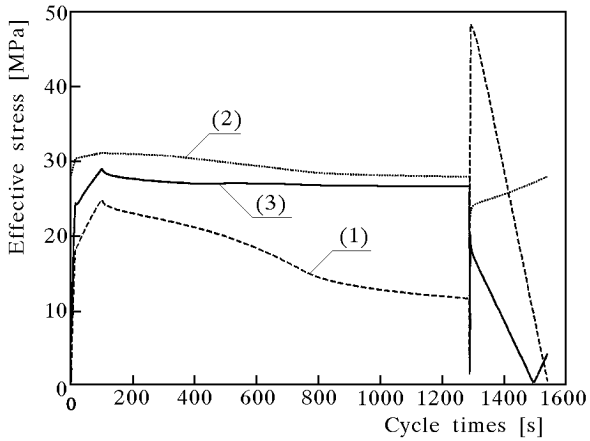

Fig. 8. Variation of effective stress over a stabilised cycle for the three locations (1) near the cooling duct, (2) near the mid-point of the quadrant, and (3) near the heating region. The results are shown for the balanced creep-cyclic plasticity damage cycle with an average applied stress of 25 MPa at the minimum section

Figure 8 shows the variation of effective stress with time for a stabilised cycle at points (1) near to the cooling duct (location A in Fig. 1), (2) at the centre of the quadrant and (3) near the heating radius (location B in Fig. 1). The highest stress occurs at the point at which the temperature difference

between the cooling duct and heating radius is maximum, and occurs at the cooling duct. The effective stress at the quadrant mid-point remains fairly constant through the cycle at approximately 25 MPa.

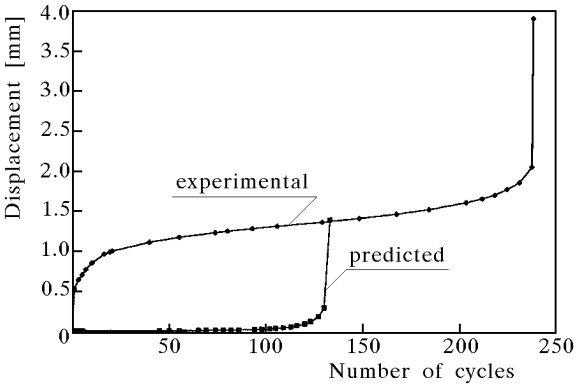

Fig. 9. Predicted and experimental variation of component loading direction displacement with cycles. The results are shown for balanced creep – cyclic plasticity-damage dominated cycle

Figure 9 shows the predicted and experimentally determined component displacement with cycles. Failure is predicted to occur at 134 cycles and is found experimentally to occur at 240 cycles. For the reasons given earlier, the model does not predict the primary ratchetting which can be seen to lead to large accumulated strains in the earlier cycles. However, the predicted steady state ratchet rates can be seen to be in reasonable agreement with the experimental data. The variations of predicted values of loading direction strain with cycles at both the cooling duct and the heating radius are shown in Figure 10. Again, the ratchet strains are largest at the cooling duct, and show a progressively increasing ratchet rate for the majority of the component life.

The levels of creep and cyclic plasticity damage at failure, (1) and (2), and at a life fraction of 0.92, (3) and (4), are shown in Figure 11a for the balanced creep-cyclic plasticity damage cycle. The levels of creep damage can be seen to be considerably higher than the cyclic plasticity damage and arises predominantly in the quadrant mid-region. Failure is again predicted to occur by the propagation of damage through the component minimum section. This is also observed to occur experimentally (Hayhurst *et al.*, 2005), as shown in Figure 11b where surface damage in the heating radius can also be seen as predicted by the model.

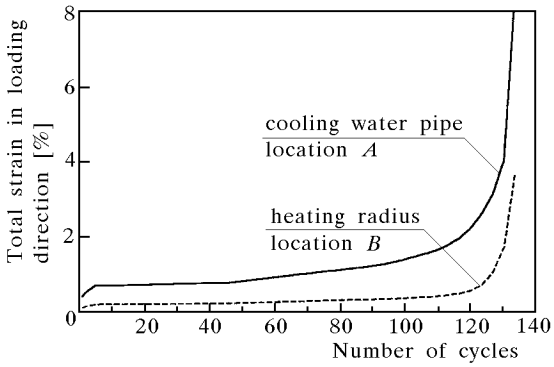

Fig. 10. Variation of total strain with number of cycle at locations A and B specified in Figure 3. The results are shown for the cyclic plasticity -dominated cycle

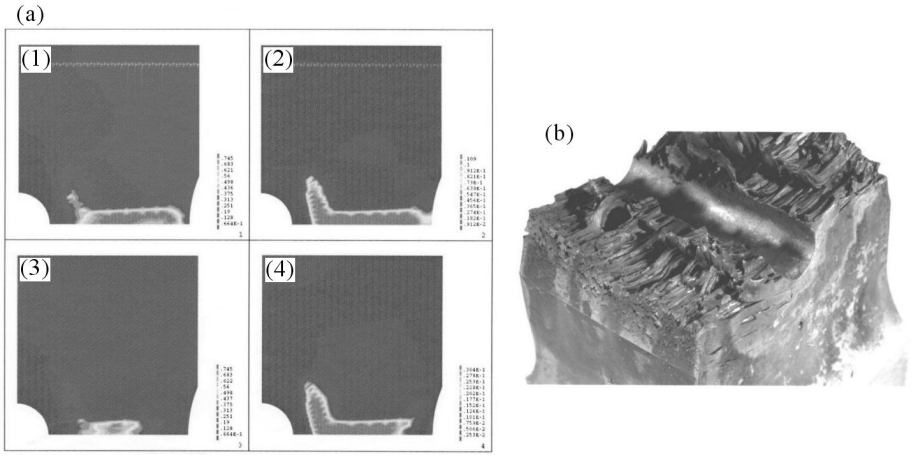

Fig. 11. (a) Predicted spatial variations of creep (1) and cyclic plasticity (2) damage at component failure and at a life fraction of 0.92, (3) and (4) respectively, shown for the balanced creep – cyclic plasticity damage-dominated cycle, and (b) failed slag tap tested under an applied average mechanical stress of 25 MPa for the balanced cyclic plasticity-dominated damage cycle showing surface damage at the external heating radius, predicted by the model

7. Conclusions

A continuum damage-based finite element model has been presented for the analysis of components suffering creep, cyclic plasticity and ratchetting due to combined cyclic thermal and mechanical loading. The model employs cycle jumping techniques to reduce computer CPU times.

Experiments have been described in which copper components have been subjected to combined cyclic thermal loading together with constant mechanical load. The resulting component ratchetting behaviour was quantified, and the components tested through to failure.

The ratchetting, failure mode and lifetimes of the components were predicted using the finite element model developed and the results compared with the experiments. Although the primary ratchetting is not predicted due to the assumption in the model of an instantaneously fully cyclically hardened state of the material, steady state ratchet rates were found to be well predicted, and lifetimes for both cyclic plasticity and balanced creep and cyclic plasticity conditions were reasonably well predicted. The mode of failure for both loading conditions was correctly predicted.

A. Damage constitutive equations

$$\dot{\varepsilon}_p = \frac{3}{2}\Big\{\frac{1}{K}\Big[\frac{J(\sigma - x)}{1 - D} - k\Big]\Big\}^n \frac{\sigma' - x'}{J(\sigma - x)} \tag{A.1}$$

$$\dot{x}_i = \frac{2}{3} C_i \dot{\varepsilon}_p (1 - D) - \gamma_i x_i \dot{p} + \frac{C_i'}{C_i} x_i \dot{\theta} \tag{A.2}$$

$$\dot{x} = \sum_{i=1}^{n} \dot{x}_i \qquad (\text{where } \; n = 2) \tag{A.3}$$

$$\dot{\omega} = A \frac{[\alpha\sigma_I + (1 - \alpha)\sigma_e]^v}{(1 - D_c)^\phi} \tag{A.4}$$

$$\frac{d\psi}{dN} = [1 - (1 - D_p)^{\beta+1}]^p \Big[\frac{A_{II}}{M(1 - D_p)}\Big]^\beta \tag{A.5}$$

$$D_c = \omega + \alpha_1 z(\omega)\psi \tag{A.6}$$

$$D_p = \psi + \alpha_2 z(\omega)\omega \tag{A.7}$$

$$D = \omega + \psi \tag{A.8}$$

$$z(\omega) = \frac{1}{2} + \frac{1}{\pi} \tan^{-1} \mu(\omega - \omega_I) \tag{A.9}$$

$$\sigma = (1 - D)E(\varepsilon - \varepsilon_p - \varepsilon_\theta) \tag{A.10}$$

in which K, n, C_i, γ_i, A, α, β, v, ϕ, p, α_1, α_2, ω_1 and μ have been determined for copper (Dunne and Hayhurst, 1992a; Lin *et al.*, 1996).

References

1. BENALLAL A., BEN CHEIKH A., 1987, Constitutive equations for anisothermal elasto-viscoplasticity, In: *Constitutive Laws for Engineering Materials; Theory and Applications*, C. Desai, E. Krempl (edit.), 607-674
2. BENALLAL A., MARQUIS D., 1987, Constitutive equations for non-proportional cyclic elasto-viscoplasticity, *J. Eng. Mater. Technol.*, **109**
3. BLACKMAN D.R., SOCIE D.F., LECKIE F.A., 1983, Applications of continuum damage concepts to creep fatigue interactions, *ASME Symp. on Thermal and Environmental Effects on Fatigue*, Portland, 45-47
4. BODNER S.R., PARTOUM Y., 1975, Constitutive equations for elasto-viscoplastic strain hardening materials, *J. Appl. Mech.*, **97**, 385-489
5. CHABOCHE J.L., 1987, Cyclic plasticity and ratchetting effects, In" *2nd Inst. Conf. on Constitutive Laws for Engineering Materials: Theory and Applications*, University of Arizona, Tucson, USA
6. CHABOCHE J.L., 1988, Continuum damage mechanics. Part II. Damage growth, crack initiation and crack growth, *J. Appl. Mech.*, **55**, 65-72
7. CHABOCHE J.L., ROUSELLIER G., 1983, On the plastic and viscoplastic constitutive equations. Part 1. Rules developed with internal variable concept, *J. Press. Vessel Technol.*, **105**, 153-158
8. DUNNE F.P.E., HAYHURST D.R., 1992a, Continuum damage based constitutive equations for copper under high temperatures creep and cyclic plasticity, *Proc. R. Soc. Lond.*, **A 437**, 454-556
9. DUNNE F.P.E., HAYHURST D.R., 1992b, Modelling of combined high temperature creep and cyclic plasticity in components using continuum damage mechanics, *Proc. R. Soc. Lond.*, **A 437**, 567-589
10. DUNNE F.P.E., HAYHURST D.R., 1994, Efficient cycle jumping techniques for the modelling of materials and structures under cyclic mechanical and thermal loading, *Eur. J. Mech.*, **13**, 5, 639-660
11. DUNNE F.P.E., MAKIN J., HAYHURST D.R., 1992, Automated procedures for the determination of high temperature viscoplastic damage constitutive equations, *Proc. R. Soc. Lond.*, **A 437**, 527-544
12. DUNNE F.P.E., PUTTERGILL D.B., HAYHURST D.R., MABBUTT Q.J., 1993, Experimental investigation of cyclic plasticity continuum damage evolution in an engineering components subjected to thermal loading, *J. of Strain Anal.*, **28**, 4, 263-272
13. GREENWOOD G., 1973, Creep life and ductility. Microstructures and the design of alloys, *Int. Conf. on Metals*, **2**, 91-98

14. HALL F.R., HAYHURST D.R., 1991, Continuum damage mechanics modelling of high temperature deformation and failure in a pipe weldment, *Proc. R. Soc. Lond.*, **A 433**, 383-403

15. HALL F.R., HAYHURST D.R., BROWN P.R., 1996, Prediction of plane strain creep-crack growth using continuum damage mechanics, *Int. J. Damage Mech.*, **5**, 353-383

16. HAYHURST D.R., 1972, Creep rupture under multi-axial states of stress, *J. Mech. Phys. Solids.*, **20**, 381-390

17. HAYHURST D.R., 1973, Stress redistribution and rupture due to creep in a uniformly stretched thin plate containing a circular hole, *J. Appl. Mech.*, **1**, 244-250

18. HAYHURST D.R., BROWN P.R., MORRISON C.J., 1984a, The role of continuum damage in creep crack growth, *Phil. Trans. R. Soc. Lond.*, **A 311**, 131-158

19. HAYHURST D.R., DIMMER P.R., MORRISON C.J., 1984b, Development of continuum damage in the creep rupture of notched bars, *Phil. Trans. R. Soc. Lond.*, **A 311**, 103-129

20. HAYHURST D.R., HAYHURST R.J., VAKILI-TAHAMI F., 2005a, CMD predictions of creep damage initiation and growth in ferritic steel weldments in a medium bore branched pipe under constant pressure at 590°C using a 5-material weld model, *Proc. R. Soc. Lond.*, **A 461**, 2303-2326

21. HAYHURST D.R., MAKIN J., WONG M.T., XU Q., 2005b, Modelling of combined creep and cyclic plasticity in a model component undergoing ratchetting using continuum damage mechanics, *Philosophical Magazine*, **85**, 16, 1701-1728

22. INOUE T., IGARI T., YOSHIDA F., SUZUKI A., MURKAMI S., 1985, Inelastic behaviour of 2.25Cr-1Mo steel under plasticity-creep interaction conditions, *Nucl. Eng. Des.*, **90**, 287

23. KUJOWSKI P., MRÓZ Z., 1980, A viscoplastic material model and its applications to cyclic loading, *Acta Mechanica*, **36**, 213-130

24. JOHANSSAN G., EKH M., RUNESSAN K., 2005, Computational modelling of inelastic large ratchetting strains, *Int. J. Plasticity*, **21**, 5, 955-980

25. LEMAITRE P.M., CHABOCHE J.L., 1990, *Mechanics of Solid Materials*, Cambridge University Press

26. LEMAITRE P.M., PLUMTREE A., 1979, Applications of damage concepts to predict creep-fatigue failure, *J. Eng. Mater. Technol.*, **101**, 284-292

27. LESNE P.M., CHABOCHE J.L., 1984, Predictions of crack initiation under thermal fatigue and creep, In: *2nd Int. Conf. on Fatigue and Creep, Fatigue 84*, Birmingham, UK

28. LIN J., DUNNE F.P.E., HAYHURST D.R., 1996, Physically-based temperature dependence of elasto-viscoplastic constitutive equations for copper between 20 and 500°C, *Philos. Mag.*, **74**, 2, 359-382

29. LIN J., DUNNE F.P.E., HAYHURST D.R., 1997, Approximate method for the analysis of components undergoing ratchetting and failure, *J. of Strain Analysis*, **33**, 1, 55-65

30. LIN J., DUNNE F.P.E., HAYHURST D.R., 1999, Aspects of testpiece design responsible for errors in cyclic plasticity experiments, *Int. J. of Damage Mechanics*, **8**, 2, 109-137

31. LIU M.C.M., KREMPL E., 1979, A uni-axial viscoplastic model based on total stress and overstress, *J. Mech. Phys. Solids*, **7**, 377-391

32. MANONUKUL A., DUNNE F.P.E., KNOWLES D., WILLIAMS S., 2005, Multiaxial creep and cyclic plasticity in nickel-base alloy C263, *Int. J. of Plasticity*, **21**, 1-20

33. MILLER A., 1979, An inelastic constitutive model for monotonic cyclic and creep deformation. Part 1. Equations development and analytical procedures, *J. Eng. Mater. Technol.*, **98**, 97-105

34. REMY L., SKELTON P., 1990, Damage assessment of component experiencing thermal transients, In: *Proc. Int. Conf. on High Temp. Structural Design*, CEC, Venice. Bury St Edmunds: MEP

35. WANG Z.P., HAYHURST D.R., 1994, The use of super-computer modelling of high temperature failure in pipe weldments to optimise weld and heat affected zone material property selection, *Proc. R. Soc. Lond.*, **A 446**, 127-148

Modelowanie pełzania, ratchetingu[1] oraz zniszczenia elementów konstrukcyjnych poddawanych obciążeniom termo-mechanicznym

Streszczenie

W pracy przedstawiono doświadczenia, w których miedziane elementy poddawano złożonym obciążeniom zawierającym cykle termiczne i obciążenia stałe. Zastosowano dwa cykle termiczne prowadzące do uszkodzenia z przewagą cyklicznej plastyczności i zrównoważonego pełzania oraz cykle obciążeń wywołujących uszkodzenie typowe dla cyklicznej plastyczności. Obciążenia złożone wywoływały ratcheting badanych elementów, a w efekcie końcowym zniszczenie. Techniki metody elementów

[1]W literaturze polskiej stosuje się ten termin bez tłumaczenia, gdyż brak jest jednego określenia na przyrostowe narastanie odkształceń pod wpływem przyłożonego obciążenia

skończonych kontynualnej mechaniki uszkodzeń zostały rozwinięte dla cyklicznej plastyczności w złożonym stanie naprężenia, pełzania oraz ratchetingu w elementach poddawanych obciążeniom termo-mechanicznym. W sformułowaniu metody elementów skończonych, aby zminimalizować czasy centralnego procesora (CPU) komputera, zastosowano techniki skoków cyklicznych. Metody elementów skończonych zastosowano w przewidywaniu zachowania się elementów miedzianych wcześniej badanych doświadczalnie, a otrzymane wyniki porównano. Zaproponowane modele w sposób satysfakcjonujący pozwalają przewidywać prędkości stanu ustalonego ratchetingu. Także przewidywania dotyczące sposobów zniszczenia oraz żywotności badanych elementów są zadowalające. Wyniki doświadczalne pokazują istotny wpływ izotropowego wzmocnienia cyklicznego na początkowe składowe prędkości ratchetingu.

Manuscript received August 22, 2005; accepted for print March 15, 2006